de Vries liquid crystals based on a chiral 5-phenylpyrimidine benzoate core with a tri- and tetra-carbosilane backbone

S. P. Sreenilayam, D. Rodriguez-Lojo, D. M. Agra-Kooijman, J. K. Vij, V. P. Panov, A. Panov, M. R. Fisch, Satyendra Kumar, and P. J. Stevenson

Phys. Rev. Materials **2**, 025603 — Published 26 February 2018

DOI: 10.1103/PhysRevMaterials.2.025603

De Vries liquid crystals based on chiral 5-phenylpyrimidine benzoate core with tri- and tetra- carbosilane backbone

S. P. Sreenilayam,[1] D. Rodriguez-Lojo,[2] D. M. Agra-Kooijman,[3] J. K. Vij,[1*] V. P. Panov,[1] A. Panov,[2] M. R. Fisch,[4] Satyendra Kumar,[5] and P. J. Stevenson[2]

[1]Department of Electronic and Electrical Engineering, Trinity College Dublin, The University of Dublin, Dublin 2, Ireland
[2]School of Chemistry and Chemical Engineering, Queens University, Belfast BT7 1NN, UK
[3]Liquid Crystal Institute, Kent State University, Kent, Ohio 44242, USA
[4]College of Aeronautics and Engineering, Kent State University, Kent, Ohio 44242, USA
[5]Division for Research and Department of Physics, University at Albany, New York 12222, USA

New chiral de Vries smectic liquid crystalline compounds are designed, synthesized and investigated for perspective applications in defect - free bistable surface stabilized ferroelectric liquid crystal (SSFLC) displays. In these compounds, a 5-phenyl-pyrimidine benzoate core is terminated on one side by a tri/tetra carbosilane group linked through an alkoxy group and alkyl spacer and the opposite side terminated by chiral 2-octanol group. The stereogenic centre contains either a methyl or perfluoromethyl functional group. These compounds exhibit Iso - SmA* - SmC* - SmX - Cr phases under cooling from the isotropic state. Measurements of the temperature dependent smectic layer spacing by x-ray diffraction experiments combined with the measured apparent optical tilt angle and the birefringence reveal that SmA* phase in these compounds is of the de Vries type. In addition, the chiral compound with a tetracarbosilane backbone, **DR277**, reported for the first time, exhibits good de Vries properties with the SmC* phase exhibited over a wide temperature range. By varying the carbosilane end group, the de Vries properties are enhanced, that is the layer shrinkage of ~ 1.9 % for the tricarbosilane **DR276** is reduced to ~ 0.9 % for tetracarbosilane **DR277** at 10 °C below SmA* to SmC* transition temperature, T_{AC}. For **DR277**, reduction factor $R \approx 0.22$ for $T = (T_{AC} - 10)$ °C is reasonably low and optical tilt angle $\theta_{App} = 35.1°$ hence this compound is a 'good de Vries smectic' LC. Therefore, synthesis of the chiral mesogen with even a higher number of carbosilane groups may lead to a further reduction or even zero layer shrinkage exhibited at T_{AC} with SmC* phase extending over a wide temperature range at room temperature for perspective suitability in device applications. Our results for 5-phenyl-pyrimidine benzoate core based compounds support a recently drawn conclusion by Schubert *et. al.* J. Mater. Chem. C 4, 8483 (2016) from a different compound, that a carbosilane backbone in chiral mesogens strongly influences the de Vries properties.

*Author of correspondence, email: jvij@tcd.ie

Introduction

Liquid crystal (LC) devices based on ferroelectric smectics display much faster switching speeds (usually of the order of a few microseconds) compared to currently used nematic LCs where the switching speed is slow and is of the order of a few milliseconds [1]. It is therefore essential to explore ferroelectric smectics for the next generation of devices. In most chiral ferroelectric smectic LCs, an emergence of the molecular tilt at the SmA* - SmC* transition leads to a contraction of the smectic layer spacing under cooling (Fig. 1a). This layer contraction combined with the surface anchoring of constituent molecules leads to an irreversible transformation from bookshelf to chevron structures. In the latter, the layer structures fold themselves in opposite directions; these opposite folds create zigzag defects in the texture of a LC cell, thus degrading the quality of devices and severely limiting their uses for a successful commercialization of ferroelectric LC displays [2-4]. An immediate solution is to avoid this problem altogether by developing new chiral LCs with a minimal layer-shrinkage at the SmA*- SmC* transition temperature as well as within SmC* phase.[4]

The first experimental observation of smectic liquid crystals having the same layer spacing in both SmC and SmA phases was made by Diele *et al.* in 1972 in Halle [5]. They also found that the layer spacing d in these materials was actually much lower than the length of the molecule L in its most extended configuration. Based on the layer-spacing results and on having determined that SmA to SmC phase transition in these materials is of first-order, de Vries proposed in 1977 that in these materials the tilt angle in the SmA phase is not zero as had generally been assumed [6]. This unusual behaviour was originally explained by the diffuse cone model (Fig. 1b) in which molecules in the SmA phase have a tilted orientation and these tilt directions are disordered in azimuthal (φ) angle [7, 8] According to this model, SmA - SmC phase transition is affected by ordering of φ to a specific tilt direction with a certain value. This explains as to why the SmA - SmC transition is first order with zero layer contraction. These observations were made when most smectic LCs were formed from achiral molecules. If we introduce chirality, then these phases are denoted by SmA* and SmC*. This special class of chiral smectics possess a large field induced electroclinic effect (linear dependence of the induced apparent tilt angle θ_{App} on a weak applied electric field E) [9, 10] (Fig. 1c), large molecular fluctuations especially in the tilt [11-13] and a significantly large increase in the birefringence with the electric field especially at the SmA* - SmC* transition [14, 15].

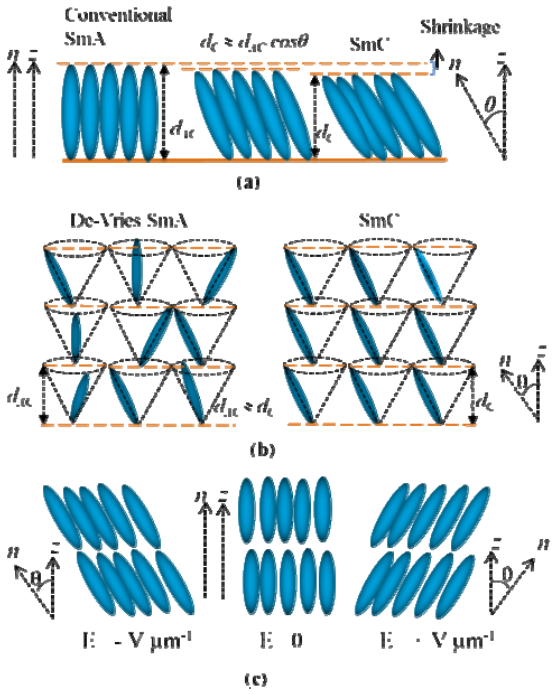

Fig. 1 Schematic representation of the molecular arrangements in SmA and SmC phases in accordance with (a) conventional model for smectic A and C phases and, (b) de Vries diffuse-cone model and (c) the demonstration of the electroclinic effect in a SmA* phase. z is the layer normal, n is the average direction of the molecular long axis orientation, θ is the angle between n and z, d_C and d_A are the layer spacings in SmC and SmA, whereas d_{AC} is the layer spacing at the SmA to SmC phase transition temperature T_{AC}.

Several chiral and non-chiral LC materials have recently been found to exhibit maximum layer shrinkage ranging from 0.2% to 1.7% [10, 16-22] or in some cases extremely low layer shrinkage at the SmA - SmC transition is displayed [14]. Among the siloxane terminated non-chiral materials, mesogen **3(n)** (Fig. 2a) shows good de Vries - like properties [19] and undergoes SmA to SmC phase transition with a layer shrinkage ranging from 0.5% to 1.4% which is rather low. The tricarbosilane **QL32-6**, a chiral analogue of mesogen **3(n)** shows a low layer contraction of only 0.2% upon phase transition from uniaxial SmA* to the tilted SmC* phase [18]. The siloxane terminated **TSiKN65** [15] (Fig. 2b) and its carbosilane analogue **W599** [23] (Fig. 2b) are amongst the best chiral de Vries LCs reported to date since these materials undergo a first order SmA* to SmC* phase transition on cooling where the layer shrinkage is < 1%. The transition is accompanied with a large increase in the birefringence with applied electric field. Also, these compounds exhibit remarkably high electroclinic susceptibilities, *i.e.* the apparent tilt angles for electric fields < 5 V/µm and for (T - T_{AC})= +1°C are 31° and 25°, respectively. These compounds are based on nitro biphenyl benzoate core, terminated by chiral alkyloxy chain on one side and terminated by the siloxane or carbosilane alkoxy chain on the opposite side (Fig. 2b).

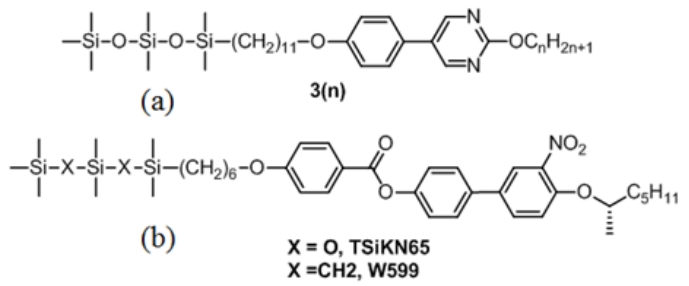

Fig. 2 Molecular structures of (a) **3**(**n**), [19] and (b) **TSiKN65**/ **W599** [15, 23].

With these structures in mind, we have designed a series of compounds with 5-phenylpyrimidine benzoate core (Fig. 3) to explore properties of mesogens that combine functional groups present in some of the most remarkable de Vries materials but with a different core of the mesogen [19, 15, 23]. The studied molecules are structurally related to each other. These have the same aromatic core and carbosilane backbone on one side. In particular, it is found that the carbosilane group promotes SmC behaviour whereas 5-phenylpyrimidine promotes SmA. The latter can generally be regarded as the SmA promoting element. Carbosilane based materials **ADPD003** and **DR253** are terminated by alkyloxy chain involving chiral CF_3 on the opposite end of the core. However, in **DR276** and **DR277,** CF_3 group is replaced by CH_3 group. The only difference between **DR277** and the tricarbosilane **DR276** is the addition of one more carbosilane group, *i.e.* it contains tetracarbosilane backbone. An ester group in the mesogen core increases the polarity of the molecule and the chiral centre is responsible for inducing chiral smectic phases. The transition temperatures with the enthalpy of transitions and phases of the studied compounds using DSC are given in the Table 1.

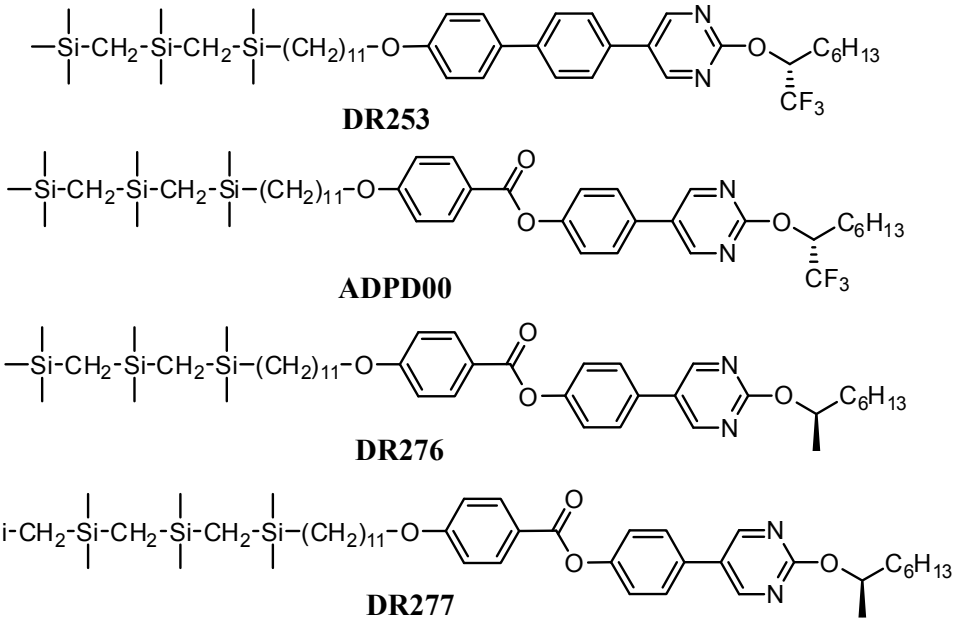

Fig. 3 Molecular structure and names of the compounds under investigation

Table 1 Mesophases with transition temperatures that have experimentally been determined as stated in the text. Transition enthalpies ΔH [in J/g] are detected on second cooling carried out at the rate of 10 °C min^{-1} by differential calorimetry (DSC). Mesophase transitions are also investigated using polarizing optical microscope (POM). The symbols: Iso. and Cr. stand for the isotropic liquid and the solid crystal states.

LC Material	**Mesophases and transition temperatures with transition enthalpies [ΔH in J/ g] under cooling**
DR253	Cr 50.2 °C [-15.3] Iso
ADPD003	Cr 52 °C [-26.7] Iso
DR276	Cr 14°C [-23.7] SmX 48°C [-] SmC* 78.5°C [-0.4] SmA* 87°C [-2.7] Iso
DR277	Cr 6°C [-17.3] SmX 35°C [-] SmC* 65.5°C [-0.4] SmA* 77°C [-1.1] Iso

The main objective of this study is to develop de Vries LCs for bistable SSFLC displays that exhibit defect - free behaviour. These are made possible by investigating the de Vries properties by systematically varying length of the carbosilane tail. In de Vries scenario, the LC molecules in the SmA* phase are already tilted in the absence of electric field. Application of the electric field only orders the azimuthal directions of the tilt, such that in doing so, the field does not induce any layer contraction and thereby avoids chevron defects from appearing in the texture. This work reports the design, synthesis and characterization of carbosilane terminated smectic materials denoted as **DR253, ADPD003, DR276,** and, **DR277**. The molecular design involves two elements: carbosilane tail that promotes SmC and 5-phenylpyrimidine that promotes SmA. Liquid crystalline phase transitions are investigated by using differential scanning calorimetry (DSC), polarized optical microscopy (POM), x-ray diffraction (XRD).The electro-optical studies include results of birefringence and the apparent tilt angle. In this paper, we investigate ferroelectric properties, electroclinic effect and the corresponding 'de Vries-like' behavior in the carbosilane terminated **DR276** and **DR277** mesogens. In 2014, Mulligan *et al*. studied the effect of varying the length of the carbosilane end group on de Vries properties of a non-chiral LCs with chloro terminated alkoxy chains [22]. They reported that de Vries properties in 5 phenyl -1,3,4-thiadiazole achiral mesogen are enhanced with an increase in the length of the end group: from monocarbosilane to tricarbosilane. So far, no other compounds have been reported in the literature with a further increase in the carbosilane chain length from the tricarbosilane tail. Therefore, for drawing a comparison we have synthesized chiral materials with tri- and tetra- carbosilane attachments and these are studied here in detail. Herein, we discuss the effect of varying length of carbosilane tail from tri- to tetra- on de Vries properties in the chiral 5-

phenylpyrimidinebenzoate mesogen. The tetracarbosilane terminated mesogen **DR277** undergoes SmA* -SmC* transition with a maximum layer contraction of only 0.9 % in the SmC* phase and a reduction faction *R* of ~ 0.222 relative to its thickness at the SmA*- SmC* transition temperature, T_{AC}. These parameters suggest that DR277 is one of the best chiral de Vries smectics.

Experimental

I. Material synthesis

The chiral mesogen **DR253** was formed following the synthetic approach as shown in Scheme 1. Nucleophilic aromatic substitution of 5-bromo-2-chloropyrimidine with a fluorinated chiral alcohol gave **1**. 11-Bromoundec-1-ene was hydrosilylated with ((dimethylsilyl)methyl)-dimethyl((trimethylsilyl)methyl)silane (prepared as described)[24] under standard conditions using Karstedt's catalyst to form a silyl terminated bromide chain. An S_N2 substitution of the silylated bromide with 4-bromo-4'-hydroxybiphenyl in basic media led to compound **2** in 82% yield. From this boronic acid **3** was formed from **2** using standard conditions of ^{t}BuLi and trimethylborate at -78 ^{o}C. A Suzuki cross coupling was used to combine the fragments **1** and **3** leading to **DR253** in 51% yield.

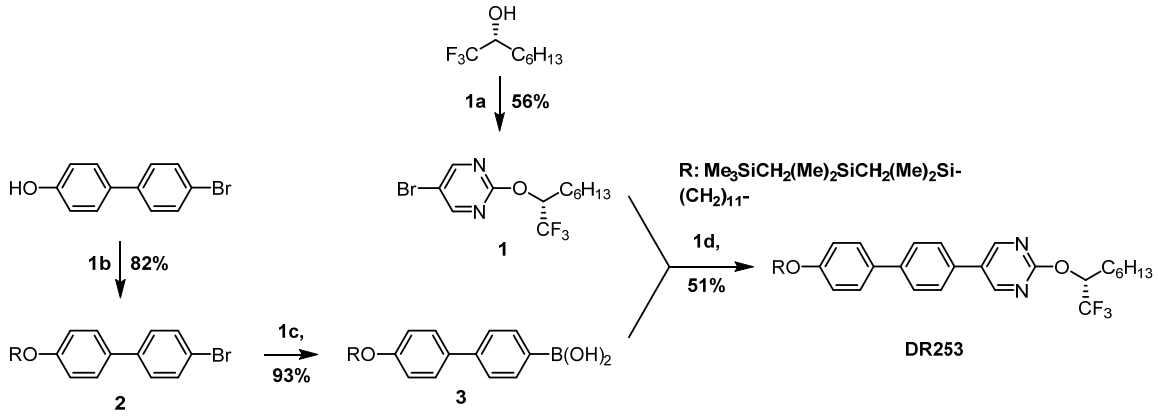

Scheme 1. *Reagents and conditions*: (1a) Na, Toluene, 50 ^{o}C (1b) $Me_3SiCH_2(Me)_2SiCH_2(Me)_2Si\text{-}(CH_2)_{11}\text{-}Br$, K_2CO_3, DMF, 80 ^{o}C; (1c) ^{t}BuLi, $B(OMe)_3$, THF, -78 ^{o}C; (1d) $Pd(PPh_3)_4$, $K_2CO_{3(aq)}$, Toluene/MeOH, reflux.

The chiral mesogen **ADPD003** was prepared following the synthetic approach shown in Scheme 2. The afore mentioned silyl terminated bromide was substituted with methyl 4-hydroxybenzoate in basic media. The ester was then hydrolysed using sodium hydroxide under reflux giving acid **4** in 72% yield over the 2 steps. Suzuki cross coupling of 4-hydroxyphenylboronic acid with aryl bromide **1** gave product **5** in 51% yield. The acid **4** and

phenol **5** were condensed using *N,N′*-dicyclohexylcarbodiimide, DCC to give the final product in 52% yield.

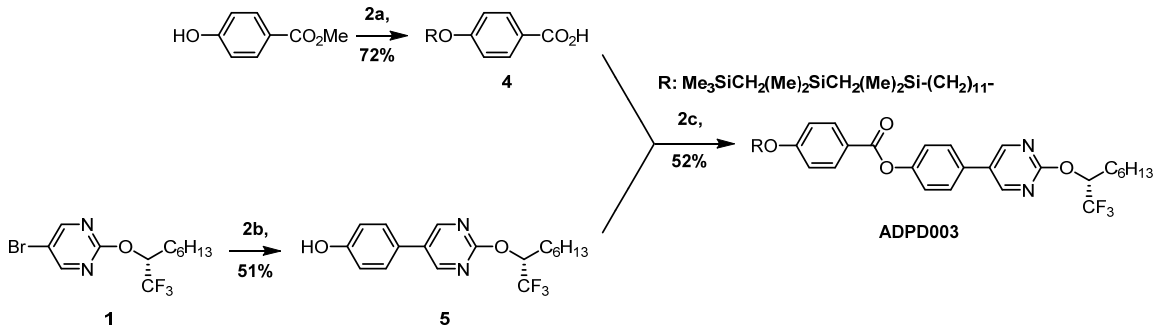

Scheme 2. *Reagents and conditions*: (2a) 1.) $Me_3SiCH_2(Me)_2SiCH_2(Me)_2Si\text{-}(CH_2)_{11}\text{-}Br$, K_2CO_3, DMF; 2.) NaOH, EtOH/H_2O, reflux; (2b) 4-hydroxyphenylboronic acid, $Pd(PPh_3)_4$, $K_2CO_{3(aq)}$, Toluene/MeOH, reflux; (2c) DCC, DMAP, DCM.

The compounds **DR276** and **DR277** were prepared following the synthetic approach shown in Scheme 3. The first step was a S_N2 displacement of 11-bromoundec-1-ene with ethyl 4-hydroxybenzoate in basic media followed by treatment with LiOH in MeOH/H_2O which led the carboxylic acid **6** in 86% yield. Suzuki cross coupling of (4-hydroxyphenyl)boronic acid and pyrimidine ether **7** gave pyrimidine **8** in 59% yield. Coupling of **6** and **8** using DCC and DMAP in DCM led to the ester **9** in 82% yield. **DR276** was prepared by hydrosilylation of the alkene **9** using ((dimethylsilyl)methyl)dimethyl-((trimethylsilyl)methyl)silane and platinum(0)-1,3-divinyl-1,1,3,3-tetramethyldisiloxane as catalyst in 56% yield. The same conditions were used for **DR277** except the silane used was 2,2,4,4,6,6,8-heptamethyl-2,4,6,8-tetrasilanonane in 43% yield.

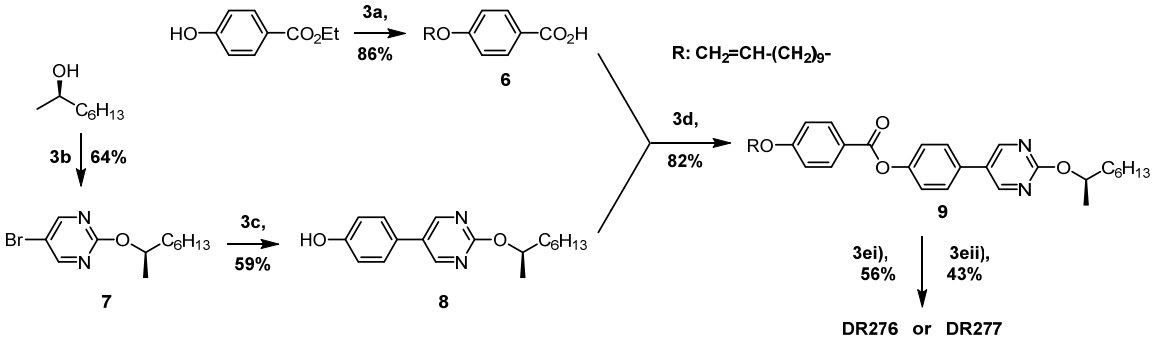

Scheme 3. *Reagents and conditions*: (3a) 1.) 11-bromoundec-1-ene, K_2CO_3, DMF; 2.) LiOH, MeOH/H_2O, reflux; (3b) Na, Toluene, 55 ^oC; (3c) (4-hydroxyphenyl)boronic acid, $Pd(PPh_3)_4$, $K_2CO_{3(aq)}$, Toluene/MeOH, reflux; (3d) DCC, DMAP, DCM; (3ei) Karstedt's catalyst, $Me_3SiCH_2(Me)_2SiCH_2(Me)_2SiH$, THF; (3eii) Karstedt's catalyst, $Me_3SiCH_2(Me)_2SiCH_2(Me)_2SiCH_2(Me)_2SiH$, THF.

2. Experimental Techniques and Measurements: Calorimetry, Electro-optical studies and X-ray diffraction

Differential Scanning Calorimetry (Perkin-Elmer DSC-7 calorimeter) is initially used to characterize the Smectic LCs studied here, where the phase transition is investigated by the enthalpy change at the transition temperature/s. The technique effectively measures a change in the heat capacity of a material as a function of temperature by comparing it with a standard reference material. Measurements are carried out under both cooling and heating cycles at a rate of 10 ^{o}C min^{-1}. It is emphasized here that heating and cooling rate of 10 ^{o}C min^{-1} is actually a fairly fast scanning rate and for this reason alone results of very small enthalpies of transitions may be somewhat inaccurate. Furthermore this may also introduce significant hysteresis in transition temperatures between the cooling and heating runs.

The electro-optical studies are carried out on planar-aligned cells with parallel rubbed polyimide alignment layer KSRP-XX/D611P6NSS05 purchased from EHC, Japan. The LC cells are studied using Olympus BX 52 polarizing optical microscope (POM), equipped with a hot stage. The latter is connected to a temperature controller, Eurotherm 2604.

X-ray diffraction (XRD) experiments were carried out using a Rigaku Screen Machine. This unit has a microfocus sealed x-ray tube with a copper anode that generates x-rays at a wavelength of λ = 1.5418 Å. X-rays are incident on the sample contained in a flamed sealed quartz capillary (1.0 mm diameter, wall thickness 0.01 mm) and the diffracted x-ray patterns are recorded by a Mercury 3 CCD detector with a resolution of 1024 × 1024 pixels; pixel size of 73.2 μm × 73.2 μm. The detector was positioned at a distance of approximately 77 mm from the sample to cover the observable length scale characteristics of the molecular system with dimensions ranging from 3.4 to 60 Å. The sample capillary was mounted in a Linkam HFS350-CAP hot-stage with a temperature controlled oven with a temperature stability of ± 0.05 °C. A built-in pair of Samarium Cobalt rare earth magnets was placed between the capillary mount to aid the orientation of the LC molecules. The sample temperature was controlled with the Linksys32 software [25] installed in the computer system used for data collection. All scans were calibrated against a Silver Behenate standard and the background scattering is subtracted (scattering from the empty capillary in the same sample position) before the data were analyzed with the aid of FIT2D software [26] and Mathematica^{TM}. Smectic layer spacing was determined from the position of the main Bragg reflection peaks.

Results and Discussion

1. Differential Scanning Calorimetry (DSC) and Polarizing Optical Microscopy (POM)

The DSC thermograms of compounds **DR253** (see Fig. S1a in ESI) and **ADPD003** (see Fig. S1b in ESI), are shown to exhibit first order transitions on cooling from the isotropic

liquid to the crystalline state with enthalpy change (ΔH) of -50 Jg^{-1} at 52°C and -26.4 Jg^{-1} at 52°C, respectively. The phases and the transition temperatures are confirmed using POM (see Fig. S2 and S3 in ESI).

Figure 3a shows DSC thermogram of the material **DR276**, 5-phenyl-pyrimidine benzoate core, terminated on one side by tricarbosilane backbone, and on the opposite by the chiral alkyloxy chain involving CH_3 group. On cooling the sample from the isotropic to SmA*, a first order phase transition is observed at temperature ~ 87 °C with an enthalpy (ΔH) change of ~ -2.7 Jg^{-1}. SmA* phase was characterized by the observations of focal conic fan-shaped texture in a 9 µm planar-aligned cell in a polarizing optical microscope (POM) (Fig. 4b); and optically uniaxial dark texture is seen in a 4.3 µm homeotropically-aligned cell (Fig. 3e) under POM.[27] On a further reduction of temperature, the material undergoes a weakly first order SmA* to SmC* phase transition at a temperature ~ 78.5 °C with a transition enthalpy ΔH ~ - 0.4 Jg^{-1}.The POM textures for the phase transition are shown in Figs. 3c and 3f. SmC* phase is distinguished from SmA* by the observation of a change in the optical texture. Fan-shaped texture characteristic of SmA* on cooling to the SmC* leads a broken fan shaped texture seen in Fig. 3c in a planar-aligned cell, the latter texture is characteristic of SmC*. The dark texture of SmA* in a homeotropic-aligned cell arises as LC molecules are oriented normal to the substrates; this changes to Schlieren texture on transition from SmA* to SmC* (Fig. 3f). For a conventional SmA* - SmC* phase transition, the tilt angle stays at the zero value in SmA* phase down to the transition temperature T_{AC}, the DSC thermogram usually exhibits a second order transition with a step in the baseline without showing a peak for the enthalpy of transition, however a change in the heat capacity is observed.[29] On lowering the temperature again, a monotropic SmX is formed, distinguished by POM texture of a homeotropically - aligned cell (Fig. 4g). In DSC thermogram, SmA* to SmX phase transition is observed to be of second order without showing any enthalpy at the transition.

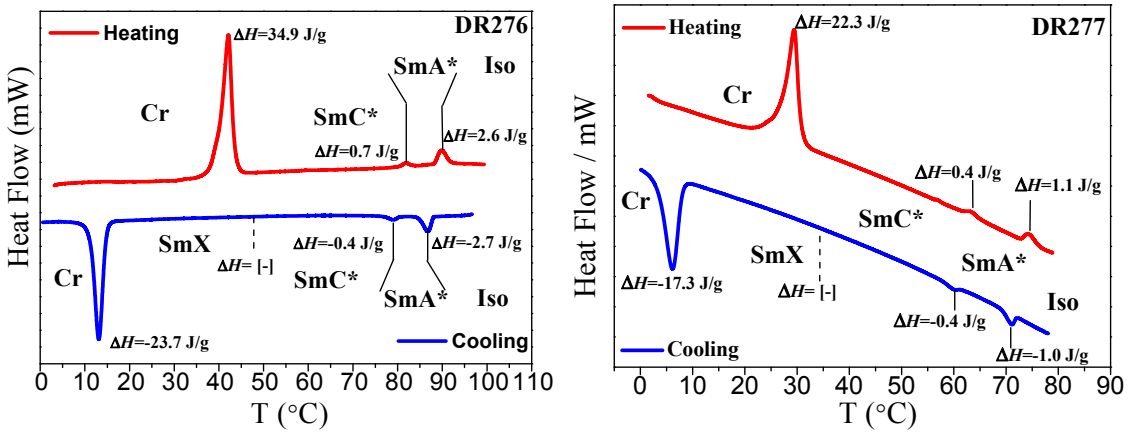

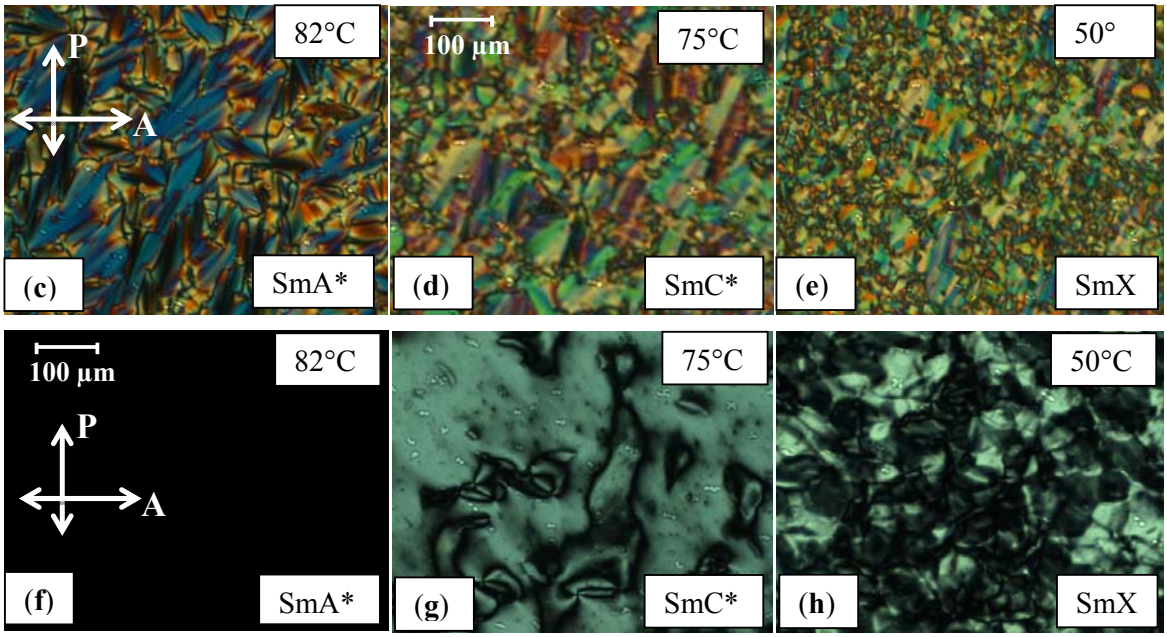

Fig. 4 Differential scanning thermograms (DSC) of (a) **DR276** and (b) **DR277**. The first cooling and second heating thermograms are obtained by ramping the temperature at a rate of 10 °C min^{-1}; continuous mesophase transitions without visible enthalpy are indicated by dashed lines. The POM images of mesophases observed in **DR276**; (c-h) under crossed polarized conditions, textures are recorded as (c – e) for a planar - aligned (cell of thickness d = 9 µm) and as (f – h) for a homeotropically – aligned cell (d = 4.3 µm). Textures are recorded under cooling cycles, (c) and (f): SmA* phase at 82 ^{o}C, (d) and (g): SmC* phase at 80 ^{o}C, and (e) and (h): SmX phase at 50 ^{o}C; SmX is not characterized/identified here.

A representative DSC plot of **DR277**, in which 5-phenyl-pyrimidine benzoate core terminated by tetracarbosilane on one side and on the opposite by chiral alkyloxy chain with CH_3 group (structure given in Fig. 3) is shown in Fig. 4b. This under cooling exhibits three transition peaks. Similar to the tricarbosilane **DR276**, this tetracarbosilane smectic shows a first order isotropic to SmA* transition with ΔH ~-1.0 Jg^{-1} at a temperature of ~ 77 ^{o}C. On lowering the temperature, the compound undergoes a weakly first order SmA* to SmC* transition with ΔH of ~-0.4 Jg^{-1} at 65.5 ^{o}C ~~[6, 27].~~ Phases SmA* and SmC* that correspond to within the transition peaks are confirmed in a planar aligned (d = 9 µm) and homeotropically aligned (d = 4.3 µm) cells using POM (see Fig. S4a, b and S5a, b in ESI). Also the monotropic SmX phase (see Fig. S4c and S5c in ESI) exhibits a second order transition without showing any enthalpy change.

During heating cycles, both compounds **DR276** and **DR277** display SmC* phase which on further heating transform to SmA* and then finally change to the isotropic state. ~~Transition temperatures are approximately the same in both heating and cooling cycles without displaying much hysteresis~~. As shown in Figs. 4a, b, on increasing the length of the carbosilane backbone

results in a gradual increase in widening the temperature range of SmA* phase. The tricarbosilane **DR276** having ~ 8.5°C wide SmA* phase shows first order crystallization transition with ΔH of ~-23.7 Jg^{-1} at a temperature of ~ 14 ^{o}C (Fig. 4a). However, an addition of one more carbosilane group in the **DR277** further widens the temperature range of SmA* to ~12.5 °C and the crystallization transition temperature is lowered to ~ 6 ^{o}C with ΔH = ~-17.3 Jg^{-1} (Fig. 4b).

A. The measurements of Birefringence (Δn), apparent tilt angle (θ_{App}) and the Polarization (P_s).

Birefringence (Δn), and the apparent optical tilt angle (θ_{App}) measurements are conducted on planar-aligned cells of **DR276** (results shown in Fig. 5a - c) and **DR277** (results shown in Fig. 6a - c) LCs, having cell thicknesses of d = 2.67 μm and 2.33 μm, respectively. Δn and θ_{App} are measured by recording the transmitted light while varying the positions of the polarizer and the analyser.[30] The experiment is performed by applying a triangular signal of 14.4 $V_{0\text{-}pk}$ μm^{-1} (f = 81.7 Hz) for **DR276** (Fig. 5a - c) and 7 $V_{0\text{-}pk}$ μm^{-1} (f = 44 Hz) for **DR277** (Fig. 6a - c). Frequencies of the applied signal are chosen to be low enough in order to allow for a sufficient time for electro-optical switching to occur while at the same time it is large enough to avoid the ionic conductivity to make a contribution to the switching current. Amplitude of the voltage applied to a planar-aligned cell of **DR276** is large enough to make θ_{App} increase slowly at first but eventually to saturate with the maximum applied electric field (Fig. 5b, c). However, for **DR277** the applied electric field is not large enough to saturate θ_{App} completely (Fig. 6b, c).

Figure 5a shows temperature dependence of Δn for **DR276** at zero field as well as for a maximum applied field of 14.4 V μm^{-1}. On cooling the planar-aligned cell of **DR276**, magnitude of the zero-field birefringence, Δn, decreases within SmA* phase with a reduction in temperature and especially dramatically closer to the SmA* - SmC* transition temperature T_{AC} (Δn = ~ 0.059). This behavior is different from that of a conventional SmA* phase where Δn increases with decreasing temperature due to an increase in the orientational order parameter. Thus, the tilt angle of the molecules in the conventional SmA* changes little with temperature and field close to the transition temperature. A continuous disorder in the azimuthal angle with increasing molecular tilt with a reduction in temperature results in Δn decreasing as temperature is lowered. As the temperature approaches SmA* - SmC* phase transition T_{AC}, the zero - field Δn suddenly increases in the SmC* followed by a slow increase with a reduction in temperature within the SmC* phase itself. This is because the azimuthal angles are ordered close to the transition but the optical tilt starts increasing with a further reduction in temperature. The

temperature dependence of Δn with applied electric field (14.4 V/μm) across a planar – aligned cell shows behavior in the SmA* phase to be entirely different from its zero-field value (Fig. 5a). Magnitude of Δn in the entire temperature range of the SmA* phase (Fig. 5a, b) now increases continuously. This is affected by reorienting the molecular azimuthal tilts through breaking the degeneracy in the azimuthal angle. An emergence of the optical tilt leads to a substantial increase in Δn with field. Thus the observed behavior is consistent with the diffuse-cone model of the SmA* with a first order SmA* - SmC* phase transition temperature (Fig. 4a). This field-induced increase in Δn in SmA* phase is in agreement with a change in the interference colors recorded by the POM at a temperature of 79.5 ^{o}C, approximately 7.5 ^{o}C below the Iso- SmA* transition temperature and 1 ^{o}C above T_{AC} (Fig. 5d-e). POM textures of a planar - aligned cell of thickness 9 μm, shown in Figs. 5d and 5e, are recorded by fixing the rubbing direction $\boldsymbol{R_d}$ at an angle of $\alpha \approx 23^{o}$ to the polarizer/analyzer direction. When placed between the crossed polarizer/analyzer, a SmA* phase at 79.5 ^{o}C in the planar –aligned cell shows a uniform dark blue color due to a finite value of Δn (Fig. 5d). An application of the external electric field, 5.5 V μm^{-1} across the planar-aligned cell shows a significant change in the color of the texture as a result of the increase in the birefringence. This is shown in Fig. 5e.

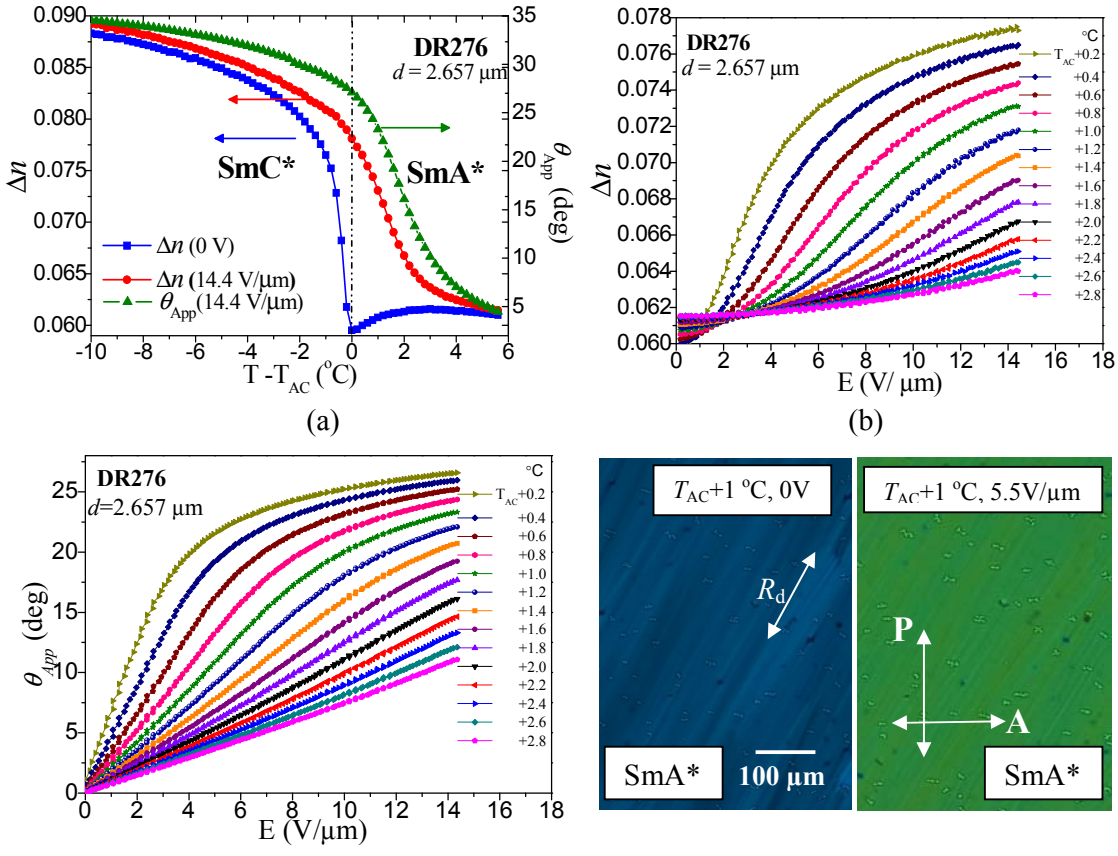

(c) (d) (e)

Fig. 5 Plots for the measured values of birefringence, Δn, and the apparent optical tilt angle, θ_{App}, for **DR276** in a 2.657 μm planar- aligned cell as a function of (a) temperature in the absence of the field and at an a.c. field of 14.4 V/ μm (f = 81.7 Hz) in SmA* and SmC* phases. Frequency is low enough that is treated close to DC but prevents ions in contributing to the results. (b) Δn and (c) θ_{App} for selected temperatures in the SmA* phase. (d) and (e) are the POM textures of SmA* phase for 0 V and 5.5 V/μm at 1°C (T_{AC} + 1°C) above the SmA* to SmC* phase transition temperature T_{AC}. Texture observations of a 9 μm planar - aligned cell under crossed polarizers are carried out by using 110 Hz square wave AC signal and by keeping the rubbing direction at an angle of α = 23° to the polarizer/analyser position.

Temperature dependencies of θ_{App} in SmA* and SmC* phases of **DR276** for a maximum applied field of 14.4 V μm^{-1} are plotted in Fig. 5a (green triangles). The dependencies of Δn (E) on temperature are also given (red circles, see Fig. 5a). Such a coupling between the θ_{App} and Δn was first proposed by Lagerwall *et al.* [31] is being demonstrated here. The dependence of θ_{App} on E is plotted in Figs. 5c in SmA* phase of DR276. The data are shown for a few temperatures only in order to avoid the figure being overcrowded. At higher temperatures in the SmA* phase where θ_{App} is low, a linear increase in θ_{App} with electric field is observed. However, in the vicinity of the SmA* - SmC* transition temperature, the electroclinic response is seen to increase dramatically and a nonlinearly in θ_{App} with E is recorded especially for $\theta_{App} > 15^o$. In the SmA* phase, close to the transition temperature T_{AC}, θ_{App} rises rapidly with the applied electric field to a value of ~ 23^o and then it increases more slowly with increasing field, finally reaching almost saturation at 26.5^o for a field of 14.4 V μm^{-1}.

Figure 6a shows temperature dependence of Δn for a planar-aligned cell of **DR277** for (i) absence of electric field and for a (ii) maximum applied E of 7 V μm^{-1}. Similar to the behavior of **DR276**, the magnitude of zero-field Δn for **DR277** is also shown to decrease within SmA* phase on cooling where a much larger drop closer to the SmA* - SmC* transition temperature T_{AC} is recorded. A comparison of the zero-field Δn values in the SmA* phase of **DR277** (zero-field Δn at T_{AC}=~ 0.048) shows relatively lower magnitude than for trisiloxane **DR277 (**zero-field Δn at T_{AC} =~ 0.059**)**. This may be due to the presence of more bulky siloxane groups in **DR277** than in **DR276.** Since the siloxane groups are more flexible and possibly exhibit more irregular conformations [15] than a bunch of hydrocarbon groups, nevertheless magnitude of Δn for both **DR276** and **DR277** in planar-aligned cells is relatively low but more so for the latter. This may be due to the shape anisotropy of the LC molecules and as a consequence increases the degree of crystallinity as being observed here in Figs. 4a, b.

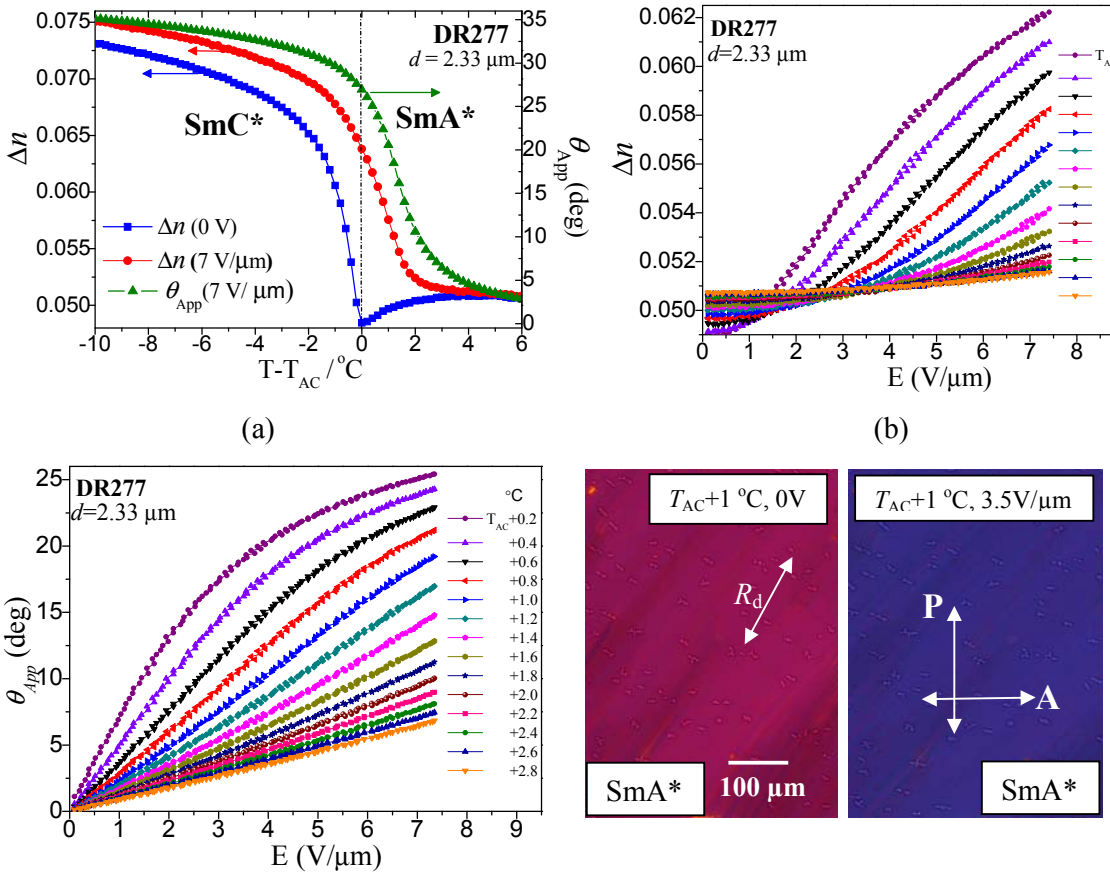

Fig. 6 Plots of Δn and θ_{App} determined as indicated for **DR277** in a planar- aligned cell of cell-thickness 2.33 µm. (a) Temperature dependencies of Δn at 0V, Δn at 7 V/ µm and θ_{App} at 7 V/µm (f = 44 Hz) in SmA* and SmC* phases. Electric field (f = 44 Hz) dependencies of (b) Δn and (c) θ_{App} for selected temperatures in the SmA* phase. (d) and (e) are the POM textures of SmA* phase for 0 V and 3.5 V/µm at 1°C (T_{AC} + 1) °C above the SmA* to SmC* phase transition temperature T_{AC}. Texture observations under crossed polarizers are made in a planar - aligned cell of cell thickness, 9 µm, by using 110 Hz square wave ac voltage and keeping the rubbing direction at an angle of α = 23° to the polarizer/analyser position.

The temperature and the electric field dependences of θ_{App} of **DR277** are shown in Fig. 6a, c. On the application of 7 V µm^{-1} electric field in SmA* phase, θ_{App} shows an increasing trend with a reduction in temperature and the magnitude of θ_{App} at (T_{AC} + 0.2) °C is ~ 26.1° (Fig. 6a). At higher temperatures in SmA* phase, we find an expected linear increase in θ_{App} with applied field (Fig. 6c) and the electroclinic response becomes nonlinear closer to the T_{AC}. Here, the applied 7 V µm^{-1} electric field is not large enough to saturate θ_{App} even at the lower temperature range of SmA* phase. 7 V µm^{-1} is the maximum field that can be applied to the sample without the samples deterioration.

The POM images of a planar - aligned cell of thickness 9 µm containing **DR277** recorded at 65.5 °C (~11.5 °C below the isotropic to SmA* transition temperature and 1 °C above T_{AC}), are shown in Fig. 6d. For texture observations, the cell is fixed in the hot stage by

keeping the LC cell rubbing direction R_d at an angle, α =~ 23° to the polarizer/analyzer. Like **DR276**, the electric field treatment at higher temperatures of **DR277** in SmA* phase closer to the isotropic phase generates a uniform mono - domain alignment. This is reasonably satisfactory for carrying out the electro-optical studies (Fig. 6). Under crossed polarizers, the SmA* phase shows a uniform pink birefringence color due to a finite value of Δ*n* (Fig. 6d) and application of an external field, 7 V μm^{-1}, produces an obvious change in the color of the POM texture (Fig. 6e), indicating an increase in the magnitude of Δ*n* (Fig. 6a, b).

In the conventional SmA* phase, LC molecules have strong orientational order even at zero- electric field. Therefore, the magnitude of Δ*n* in the absence of electric field is usually large and on the application of field, molecules stay parallel to each other in a planar-aligned cell and hence the field dependent variation of Δ*n* is very weak. By contrast, in de Vries SmA*, the LC molecules are orientationally distributed about a tilt cone in the absence of the external electric field. Therefore, on lowering the temperature from the high temperature side of SmA* phase to the SmA* - SmC* transition temperature, T_{AC}, the zero - field Δ*n* is greatly reduced due to the orientational averaging of molecules about the tilt cone. On the application of electric field, the azimuthal tilt direction becomes biased and the azimuthal angles condense to a specific value. As a result, Δ*n* of the de Vries SmA* phase should increase substantially with applied field. In the materials under study, θ_{App} and Δ*n* depend sensitively on temperature close to T_{AC}, and the electroclinic tilt (Fig. 5a, c and 6a, c) observed in SmA* phase is accompanied by the variation in the magnitude of Δ*n* (Fig. 5a, b and 6a, b). Based on the temperature and electric field dependencies of θ_{App} and Δ*n* we conclude that the SmA* phase in both **DR276** (Fig. 5) and **DR277** (Fig. 6) is of the de Vries type [32-35] and the behavior of θ_{App} and Δ*n* can be explained in terms of the de Vries diffuse cone model. [10, 23, 36].

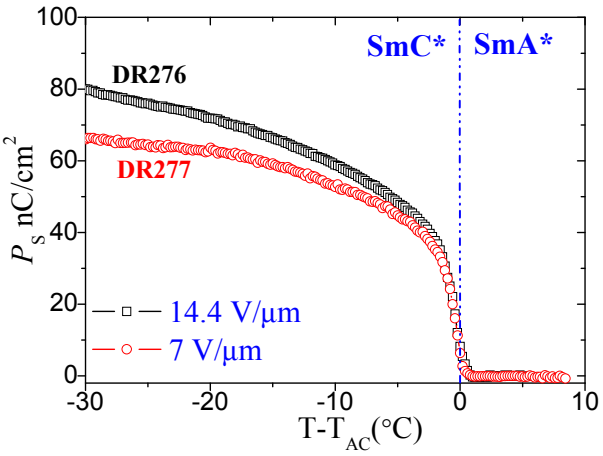

Fig. 7 Spontaneous polarization $\boldsymbol{P_S}$ *vs* (T - T_{AC}) for **DR276** (□, d = 2.657 μm, E = 14.4 V/ μm, f = 81.7 Hz) and **DR277** (□, d = 2.33 μm, E = 7 V/ μm, f = 44 Hz).

Measurements are carried out on planar - aligned cells under cooling by the application of triangular wave AC voltage.

The spontaneous polarization, $\boldsymbol{P_S}$, plots for **DR276** and **DR277** are shown in Fig. 7. Measurements are carried out on planar - aligned cells for cell-thicknesses of 2.657 µm and 2.33 µm, respectively. Values of $\boldsymbol{P_S}$ were obtained by integrating the observed current peaks recorded under the application of triangular wave voltage.[37, 38] To ensure that the polarization is saturated by the field, the amplitude of the triangular wave was selected for each sample at a maximum possible value without causing an irreversible damage to the sample (14.4 V/µm for **DR276** and 7 V/µm for **DR277**). Frequency of the waveform is optimized in SmA* phase to minimize the hysteresis arising from the viscosity and ionic effects (81.7 Hz for **DR276** and 44 Hz for **DR277**). At, $T = T_{AC} - 30$ °C, $\boldsymbol{P_S}$ for **DR276** is ~ 80 nC cm^{-2} and is ~ 66 nC cm^{-2}for **DR277**.

B. X - Ray Diffraction (XRD) studies

The XRD patterns of **DR276** in Figs. 8a, 8b and 8c show a pair of sharp arcs in the small angle scattering region corresponding to the smectic layer spacing and diffuse arcs for wide-angle scattering at 4.6 Å corresponding to the effective molecular width. The pair of arcs are orthogonal to each other in the SmA* phase (Fig. 8a) as indicated by the orthogonal solid yellow lines confirming an oriented domain in SmA* phase. At T = 67.3 °C, Fig. 8b, the arcs became wider. However, on a closer inspection, the arcs azimuthally split into several reflections for the same scattering position. This indicates tilting of the layer domains confirming the tilted SmC* phase. Because of the multiple domains, it is not possible to determine quantitatively the tilt of the molecule with respect to the smectic layer. In the low temperature mesophase below SmC* (T = 49.5 °C, Fig. 8c) assigned here as SmX, arcs appear as rings. This is consistent with diffraction patterns observed for multiple un-oriented smectic domains.

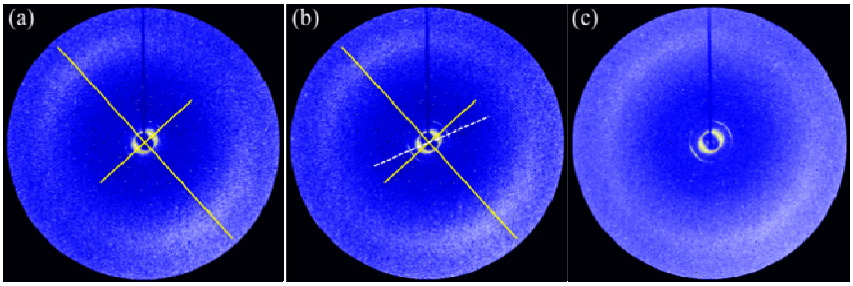

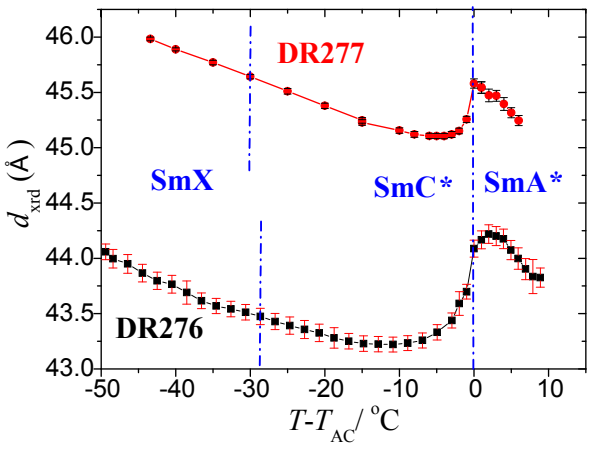

(d)

Fig. 8. X-ray diffraction patterns for **DR276** at temperatures (a) 80.1°C, (b) 67.3 °C, and (c) 49.5 °C. (d) Temperature dependence of the smectic layer spacings for **DR276** and **DR277**.

The temperature dependence of the layer spacing of **DR276**, plotted in Fig. 8d, reflects the sample undergoing a weakly first order phase transition to SmC* phase at T = 78.5 °C, as indicated by a vertical blue dashed line at T - T_{AC} = 0. At the SmA* - SmC* phase transition, the layer spacing is, d_A = (44.09 ± 0.05) Å. In the SmC* phase, the minimum layer spacing is d_C = 43.23 Å at T = 68.5 °C corresponding to T = (T_{AC} -10) °C. The optimal layer shrinkage, $\frac{d_A - d_C}{d_A} \times 100 = 1.9$ % is minimal, which is one of the important characteristics of the de Vries smectics. The increasing layer spacing at temperatures below T = 48 °C could be interpreted as the un-tilting of the molecules back to the orthogonal state (*i.e.* molecules are perpendicular to the smectic layer). However, the observed optical texture (Fig. 4g) is not consistent with this interpretation, which means this phase remains in the tilted orientation. Notably, the maximum smectic layer spacing, 44.22 Å is about 5 Å less than the molecular length (L_{calc} = 49.71 Å) in *all-trans* configuration as calculated using Avogadro (v1.1.1) [39].

The temperature dependence of the layer spacing of **DR277** is also shown in Fig. 8d. Similar to **DR276,** a weakly first order phase transition from SmA* to SmC* is observed at 65.5 °C. The maximum layer spacing occurs just above T_{AC} where d_A = 45.58 Å. The minimum layer spacing occurs at 10 °C below SmA* to SmC* T = (T_{AC} -10) °C where d_C = 45.16 Å. The optimal layer shrinkage, (d_A - d_C)/ d_A ×100 = 0.9 % is roughly one half of the value obtained for **DR276**.

The reduction factor R, a measure of de Vriesness of a smectic LC, is defined as:

$$R = \frac{\delta(T)}{\theta_{opt(T)}} = \frac{\cos^{-1}[d_c(T)/d_{AC}]}{\theta_{opt(T)}} \qquad (1)$$

where, δ (T) determines the layer contraction relative to the layer spacing d_{AC} at the SmA* to SmC* transition temperature T_{AC}. This is based on the assumption that the rigid rod model to the LCs is applicable to these materials [40]. θ_{opt} is the optical tilt angle determined using POM (Fig. 5a and 6a). According to Eq. (1), the ideal de Vries smectic LC produces a defect-free bookshelf geometry in SmC* with $R = 0$, *i.e.* the short range LC molecular tilt order at a lower temperature in the SmA* phase becomes long range close to the T_{AC}, where the de Vries cone angle is equal to the saturated θ_{opt} at $T = T_{AC}$. On entering the SmC*, the azimuthal ordering of the molecular director on the cone localizes these to a single orientation. In this case, the layer contraction is absent and then d_C (T) / d_{AC} = 1, and $R = 0$. The lowest reported magnitude of reduction factor, R, is 0.17 for the chiral de Vries **QL32-6** LC, which exhibits a maximum layer contraction of only 0.2 % at 3 K ($T = T_{AC}$-3 K) below the SmA*- SmC* transitions with θ_{opt} of 20° [18]. The molecular design of **QL32-6** combines a tricarbosilane end-group attached to a 5-phenylpyrimidine core. Even though, the **QL32-6** compound exhibits the smallest layer shrinkage, its crystallization temperature is approximately 53 °C and the SmC* phase is observed only over a temperature range of ~ 9 °C. In our case, **DR276** and **DR277** exhibit approximately 30 °C wide SmC* phase regions and their crystallization temperatures are below 15 °C. Materials **DR276** and **DR277** at 10 °C below the SmA* - SmC* transition temperature T_{AC} ($T = T_{AC}$ - 10 °C) lead to $R \approx 0.319$ and $R \approx 0.222$ and to optical tilt angles, θ_{opt} of 34.6° (Fig. 5a) and 35.1° (Fig. 6a) respectively. For **DR277**, the R value obtained is reasonably low and hence we can safely conclude that **DR277**is one of the 'best de Vries smectic' LC.

Table 2 lists the properties of **DR276** and **DR277** compounds.

Table 2 Properties of **DR276** and **DR277** compounds.

Properties	**LC Materials**	
	DR276	**DR277**
Iso-SmA* transition temperature	~ 87 °C	~ 77 °C
SmA* temperature range	~ 8.5 °C	~ 12.5 °C
SmA*-SmC* transition enthalpy (ΔH)	~ 0.4 J/g	~ 0.4 J/g
Δn at T_{AC} for $E = 0$	~ 0.059	~ 0.048
Δn at T_{AC} for $E = E_{max}$	~ 0.078 (at 14.5 V/μm)	~ 0.063 (at 7 V/μm)
Difference in Δn at T_{AC}	0.019	0.015
θ_{App} at T_{AC} + 0.2 °C	~ 26.6° (at 14.5 V/μm)	~ 26.1° (at 7 V/μm)
Layer Shrinkage at T_{AC} - 10 °C	~1.9 %	~ 0.9 %
Reduction factor, R at T_{AC} - 10 °C	~ 0.319	~ 0.222
$\boldsymbol{P_S}$ at T_{AC} - 30 °C	~ 80 nC/ cm^2 (at 14.5 V/μm)	~ 67 nC/cm^2 (at 7 V/μm)

Conclusions

The objective of our current study is to explore new, "excellent de Vries LCs", and in order to advance this objective new materials with proposed strategy have been designed and characterized. The use of various techniques such as POM, XRD, and electro-optics including measurements of birefringence confirm that these compounds indeed have characteristics of de Vries smectics. Here, we report on the synthesis and de Vries properties of a new 5-phenylpyimidine benzoate mesogen terminated with carbosilane tail on one side and the chiral 2-octanol on the opposite side. The techniques of DSC and POM are employed to determine the mesophase transition temperatures, the individual phases and find the phase transition enthalpies. Measurements of the temperature dependent smectic layer spacing combined with results of θ_{App} and Δn reveal that SmA* phase in these compounds is indeed of the de Vries type. A comparison of the two materials under study shows that the compound **DR277** with tetra carbosilane backbone exhibits better de Vries properties. We also show that by increasing length of the carbosilane tail, the layer shrinkage from ~ 1.9 % for (tri carbosilane **DR276**) is reduced to ~ 0.9 % (for tetra carbosilane **DR277)**. Our future work will involve synthesis of chiral mesogen similar to those reported here but involving even higher numbers of carbosilane groups to optimize the excellent de Vries properties observed over a wide temperature range of SmC* phase that also includes the ambient temperature. The carbosilane compounds introduced here exhibit almost ideal de Vries characteristics as do the siloxane compounds studied extensively in the literature [41-43]. However, the carbosilane compounds are relatively more stable than siloxanes with time as well as additionally easily alignable.

Conflict of interest: The authors declare no conflict of interest.

Acknowledgements

This research work was supported by 13/US/I2866 from the Science Foundation Ireland as part of the US – Ireland Research and Development Partnership program jointly administered with the United States National Science Foundation under grant number NSF-DMR-1410649. Financial support for the Belfast group was from the Department for Employment and Learning under with grant code USI 056.

References:

1 N. A. Clark, and S. T. Lagerwall, *Appl. Phys. Lett*. **36**, 899 (1980)

2 S. T. Lagerwall, *Ferroelectric and Antiferroelectric Liquid Crystals*, Wiley-VCH, Weinheim, 1999.

3 T. P. Rieker, N. A. Clark, G. S. Smith, D. S. Parmar, E. B. Sirota and C. R. Safinya, *Phys. Rev. Lett.* **59**, 2658 (1987)

4 J. P. F. Lagerwall, and F. Giesselmann, *Chem. Phys. Chem.***7**, 20 (2006)

5 S. Diele, P. Brand, and H. Sackmann, *Mol. Cryst. Liq. Cryst*. **16** 105 (1972).

6 A. de Vries, *Mol. Cryst. Liq. Cryst.* **41**, 27 (1977).

7 A. de Vries, A. Ekachai, and N. Spielberg, *Mol. Cryst. Liq. Cryst. Lett.* **49**, 143 (1979).

8 A. de Vries, *J. Chem. Phys.***71**, 25 (1979).

9 S. Garoff, and R. B. Meyer, *Phys. Rev. Lett.* **38**, 848 (1977).

10 S. P. Sreenilayam, D. M. Agra-Kooijman, V. P. Panov, V. Swaminathan, J. K. Vij, Yu. P. Panarin, A. Kocot, A. Panov, D. Rodriguez-Lojo, P. J. Stevenson, M. R. Fisch, and S. Kumar, *Phys. Rev. E* **95**, 032701 (2017).

11 N. Yadav, V. P. Panov, V. Swaminathan, S. P. Sreenilayam, J. K. Vij, T. S. Perova, R. Dhar, A. Panov, D. Rodriguez-Lojo, and P. J. Stevenson, *Phys. Rev. E* **95**, 062704 (2017).

12 H. Xu, J. K. Vij, A. Rappaport, and N. A. Clark, *Phys. Rev. Lett*. **79**, 249 (1997).

13 U. Manna, J. –K. Song, Yu. P. Panarin, A. Fukuda, and J. K. Vij, *Phys. Rev. E* **77**, 041707 (2008).

14 J. P. F. Lagerwall, F. Giesselmann, and M. D. Radcliffe, *Phys. Rev. E* **66**, 031703 (2002).

15 M. S. Spector, P. A. Heiney, J. Naciri, B. T. Weslowski, D. B. Holt, and R. Shashidhar, *Phys. Rev. E* **61**, 1579 (2000).

16 H. G. Yoon, D. M. Agra-Kooijman, K. Ayub, R. P. Lemieux, and S. Kumar, *Phys. Rev. Lett*. **106**, 087801 (2011).

17 D. M. Agra-Kooijman, H. G. Yoon, S. Dey, and S. Kumar, *Phys. Rev. E*, **89**, 032506 (2014).

18 C. P. J. Schubert, C. Müller, F. Giesselmann, and R. P. Lemieux, *J. Mater. Chem. C* **4**, 8483 (2016)

19 J. C. Roberts, N. Kapernaum, Q. Song, D. Nonnenmacher, K. Ayub, F. Giesselmann, and R. P. Lemieux, *J. Am. Chem. Soc.,* **132**, 364 (2010).

20 V. Swaminathan, V. P. Panov, Yu. P. Panarin, S. P. Sreenilayam, J. K. Vij, A. Panov, D. Rodriguez-Lojo, P. J. Stevenson and E. Gorecka, *Liq. Cryst.,* https://doi.org/10.1080-/02678292.2017.1359694, 2017.

21 S. P. Sreenilayam, D. Rodriguez-Lojo, V. P. Panov, V. Swaminathan, J. K. Vij, Y. P. Panarin, E. Gorecka, A. Panov, and P. J. Stevenson, *Phys. Rev. E* **96**, 042701 (2017).

22 K. M. Mulligan, A. Bogner, Q. Song, C. P. J. Schubert, F. Giesselmann, and R. P. Lemieux, *J. Mater. Chem. C* **2**, 8270 (2014).

23 Y. Shen, L. Wang, R. Shao, T. Gong, C. Zhu, H. Yang, J. E. Maclennan, D. M. Walba, and N. A. Clark, *Phys. Rev. E* **88**, 062504 (2013).

24 Y. Zhang, U. Baumeister, C. Tschierske, M. J. O'Callaghan and C. Walker, *Chem. Mater.* **22**, 2869 (2010)

25 http://www.linkam.co.uk/system-control-software/

26 A. P. Hammersley, S. O. Svensson, M. Hanfland, A. N. Fitch, and D. Hausermann, *High Pressure Research* **14**, 235 (1996)

27 G. W. Gray and J. W. Goodby, *Smectic Liquid Crystals*, Leonard Hill, London, 1984.

28 D. Nonnenmacher, M. A. Osipov, J. C. Roberts, R. P. Lemieux, and F. Giesselmann, *Phys. Rev. E* **82**, 031703 (2010).

29 J. W. Goodby, P. J. Collings, T. Kato, C. Tschierske, H. F. Gleeson and P. Raynes, Hand book of Liquid Crystals, Volume 1, 2nd ed.,Wiley-VCH, 2015, Ch. 3.

30 B. Park, S. -S. Seomun, M. Nakata and M. Takahashi, *Jpn. J. Appl. Phys.* **38**, 1474 (1999).

31 S. T. Lagerwall, P. Rudquist and F. Giesselmann, *Mol. Cryst. Liq. Cryst.* **510**, 148 (2009).

32 J. V. Selinger, P. J. Collings, and R. Shashidhar, *Phy. Rev. E* **64**, 061705 (2001).

33 O. E. Panarina, Yu. P. Panarin, F. Antonelli, J. K. Vij, M. Reihmann and G. Galli, *J. Mater. Chem*. **16**, 842 (2006).

34 J. P. F. Lagerwall, F. Giesselmann, and M. D. Radcliffe, *Phys Rev. E* **66**, 031703 (2002).

35 U. Manna, J. –K. Song, Yu. P. Panarin, A. Fukuda, and J. K. Vij, *Phys. Rev. E* **77**, 041707 (2008).

36 N. A. Clark, T. Bellini, R.-F. Shao, D. Coleman, S. Bardon, D. R. Link, J. E. Maclennan, X.-H. Chen, M. D. Wand, D. M. Walba, P. Rudquist, and S. T. Lagerwall, *Appl. Phys. Lett.* **80**, 4097 (2002).

37 K. Miyasato, S. Abe, H. Takezoe, A. Fukuda and E. Kuze*, Jpn. J. Appl. Phys*. **22**, L661 (1983).

38 G. Spruce and R. D. Pringle, *J. Phys. E: Sci. Instrum.* **21**, 268 (1988).

39 M. D. Hanwell, D. E. Curtis, D. C. Lonie, T. Vandermeersch, E. Zurek, and G. R. Hutchison, *J. Cheminformatics* **4**, 17 (2012)

40 Y. Takanishi, Y. Ouchi, H. Takezoe, A. Fukuda, A. Mochizuki, M. Nakatsuka, *Jpn. J. Appl. Phys.* **29**, L984 (1990).

41. N. Hayashi, T. Kato, A. Fukuda, J. K. Vij, Yu. P. Panarin, J. Naciri, R. Shashidhar, S. Kawada, and S. Kondoh. *Phys. Rev. E. 71*, 041705 (2005).

42. O. E. Panarina, Yu. P. Panarin, J. K. Vij, M. S. Spector, and R. Shashidhar, *Phys. Rev. E* 67, 051709 (2003).

43. A. Kocot, R. Wrzalik, J. K. Vij and R. Zentel, *J. Appl. Phys*. 75, 728 (1994).